Journal of Magnetism and Magnetic Materials 511 (2020) 166792

Contents lists available at ScienceDirect

Journal of Magnetism and Magnetic Materials

journal homepage: www.elsevier.com/locate/jmmm

Research articles

Novel mixed precursor approach to prepare multiferroic nanocomposites with enhanced interfacial coupling

G. Kotnana[a], F. Sayed[a], D.C. Joshi[a], G. Barucca[b], D. Peddis[c,d], R. Mathieu[a], T. Sarkar[a,*]

[a] Department of Materials Science and Engineering, Uppsala University, Box 534, SE-75121 Uppsala, Sweden
[b] Department SIMAU, University Politecnica delle Marche, Via Brecce Bianche, Ancona 60131, Italy
[c] Dipartimento di Chimica e Chimica Industriale, Università degli Studi di Genova, Via Dodecaneso 31, Genova 16146, Italy
[d] Istituto di Struttura della Materia – CNR, Area della Ricerca di Roma1, Monterotondo Scalo, RM 00015, Italy

ARTICLE INFO

Keywords:
Multiferroics
Nanocomposites
Chemical synthesis
Enhanced interfacial coupling

ABSTRACT

In the present work, we report the preparation of multiferroic $PbZr_{0.52}Ti_{0.48}O_3$ (PZT)/$CoFe_2O_4$ (CFO) nanocomposites using a new synthesis technique that can maximize the surface area of contact, and hence, the interfacial coupling between the ferroelectric (PZT) and ferrimagnetic (CFO) phases. The samples have been characterized using X-ray diffraction (XRD) and transmission electron microscopy (TEM), and the physical (magnetic and dielectric) properties have been investigated. XRD confirms the presence of the desired PZT and CFO phases in the samples without any undesired secondary phases. We also observe a reduction in the particle size of CFO in the nanocomposites as evidenced by a line broadening of the XRD reflections corresponding to the pure CFO phase. The nanocomposites show hysteresis loops and ferrimagnetic-like behaviors in their M vs H curves at room temperature, even for samples with very low fraction of the CFO phase. The coercivity of the nanocomposites is marginally larger compared to that of pure CFO, which can be due to the change in magnetic anisotropy of the CFO phase due to its reduced particle size in the nanocomposites. Room temperature polarization versus electric field measurements show a significant increase in the coercive field after the incorporation of CFO inside the PZT matrix. This work illustrates a simple, cost-effective synthesis technique that can be used to prepare nanocomposites of functional materials with desired room temperature functionalities and enhanced interfacial coupling between the two phases.

1. Introduction

Two-phase composite multiferroic materials [1–5] have been gaining increasing attention over the years, primarily because of the scarcity of single-phase multiferroic materials [6]. Two-phase composite systems open up the possibility of tailoring properties using two compounds, one ferro/ferrimagnetic and the other ferroelectric. In this context, nanocomposites are more promising than bulk materials since the former possess larger surface area leading to larger coupling between the two phases [7,8]. Our recent work on particulate magnetic nanocomposites have revealed that physical mixing of the two phases often yields nanocomposites with almost non-existent magnetic coupling between the two phases [9]. Chemical synthesis routes usually yield samples with better coupling between the two phases [10], although the extent of magnetic coupling is very much dependent on the details of the synthesis strategy [11]. In general, the extent of coupling can be related to the degree of particle agglomeration of each individual phase in the nanocomposite. Synthesis techniques that reduce the degree of particle agglomeration of each individual phase ensure maximum surface area of contact between the two phases, and thus, enhanced coupling between the two phases [11]. We have recently demonstrated this concept in bi-magnetic systems [11,12]. In the present work, we show that the same synthesis strategy can be used to prepare multiferroic nanocomposites by a proper choice of the individual components. This is expected to have a much wider application because of the possibility of enhancing the magneto-electric coupling in such nanocomposites, which can then be used for a much better control of magnetization via electric fields or polarization via magnetic fields.

The magnetic and ferroelectric components chosen in this work are $CoFe_2O_4$ (CFO) and $PbZr_{0.52}Ti_{0.48}O_3$ (PZT), respectively. CFO has a cubic spinel structure, and is a typical room temperature ferrimagnet (ordering temperature ~800 K) exhibiting high saturation magnetization, high coercivity, large magnetic anisotropy, and good chemical

* Corresponding author.
E-mail address: tapati.sarkar@angstrom.uu.se (T. Sarkar).

https://doi.org/10.1016/j.jmmm.2020.166792
Received 14 October 2019; Received in revised form 19 February 2020; Accepted 19 March 2020
Available online 20 March 2020
0304-8853/ © 2020 The Authors. Published by Elsevier B.V. This is an open access article under the CC BY-NC-ND license (http://creativecommons.org/licenses/by-nc-nd/4.0/).

stability [13]. In contrast, lead zirconate titanate, $PbZr_{1-x}Ti_xO_3$, is a prototypical room temperature ferroelectric material. It has a distorted perovskite structure below 350 °C with a ferroelectric tetragonal or rhombohedral phase and consequently shows a spontaneous polarization [14,15]. The best ferroelectric properties in this series can be obtained near the morphotropic phase boundary, where Zr:Ti = 52:48 [16]. We use these two systems to create a prototypical room temperature multiferroic nanocomposite using our novel synthesis strategy. In the following sections, we first present the details of the synthesis technique, followed by the structural, morphological, magnetic, and dielectric characterization of the nanocomposites.

2. Synthesis and experimental techniques

2.1. Synthesis

In a typical synthesis process, individual sols of CFO and PZT were prepared separately. First, 0.2 M CFO precursor solution was prepared by dissolving stoichiometric amounts of cobalt acetate tetrahydrate, $(CH_3COO)_2Co{\cdot}4H_2O$, and iron nitrate nonahydrate, $Fe(NO_3)_3{\cdot}9H_2O$, (Sigma-Aldrich) in 2-methoxyethanol (ME) and acetic acid (AA) (volume ratio of ME:AA = 7:3) at room temperature. After an initial stirring using a magnetic stirrer for ~20 min, ethanolamine was added to the solution, and the solution was stirred at room temperature for 2 h. Similarly, 0.2 M PZT precursor solution was prepared by dissolving stoichiometric amounts of lead acetate, $Pb(CH_3CO_2)_2{\cdot}3H_2O$, zirconium propoxide, $Zr(CH_2CH_2CH_3O)_4$, and titanium isopropoxide, $Ti[OCH(CH_3)_2]_4$, in 2-methoxyethanol (ME) and acetic acid (AA) (volume ratio of ME:AA = 7:3) at room temperature. Zirconium propoxide and titanium isopropoxide were added to the solution after dissolving lead acetate. Next, the solution was stirred for ~20 min, after which ethanolamine was added to the solution, and the solution was further stirred at room temperature for 2 h. After stirring the individual precursor solutions for 2 h, a mixed precursor solution was prepared by mixing the two individual precursor solutions in different volume ratios (PZT:CFO = 95:05, 75:25, and 50:50). The mixed precursor solution was first stirred at room temperature for 1 h, and then at 80 °C for 20 min. Next, the temperature was increased and maintained at ~150 °C till the formation of a gel. The temperature was then increased to ~300 °C when a self-combustion reaction occurred, yielding a fluffy powder. The powder was crushed in a mortar, transferred to a furnace, and annealed in air at 800 °C for 2 h to obtain the nanocomposite samples. Reference samples of PZT and CFO were also prepared using the individual precursor solutions of PZT and CFO by following the same steps of stirring at 80 °C and 150 °C for gel formation, and annealing at 800 °C for 2 h. The synthesis steps are summarized in Fig. 1.

2.2. Characterization techniques

The samples were characterized by X-ray diffraction (XRD) obtained using a D-5000 diffractometer with CuK_α radiation operating at 40 kV and 30 mA. The data were collected in the range 2θ = 20–70°, with a step size of 0.02°.

Transmission electron microscopy (TEM) analysis was performed using a Philips CM200 microscope operating at 200 kV and equipped with a LaB_6 filament. For TEM observations, the samples, in the form of powder, were prepared using the following procedure. A small quantity of powder was dispersed in ethanol and subjected to ultrasonic agitation for approximately one minute. A drop of the suspension was deposited on a commercial TEM grid covered with a thin carbon film; finally, the grid was kept in air until complete evaporation of the ethanol.

Magnetic field-dependent magnetization of the samples was collected using a superconducting quantum interference device (SQUID) magnetometer from Quantum Design Inc. Magnetic hysteresis loops were recorded at T = 300 K in the field range ± 5 T.

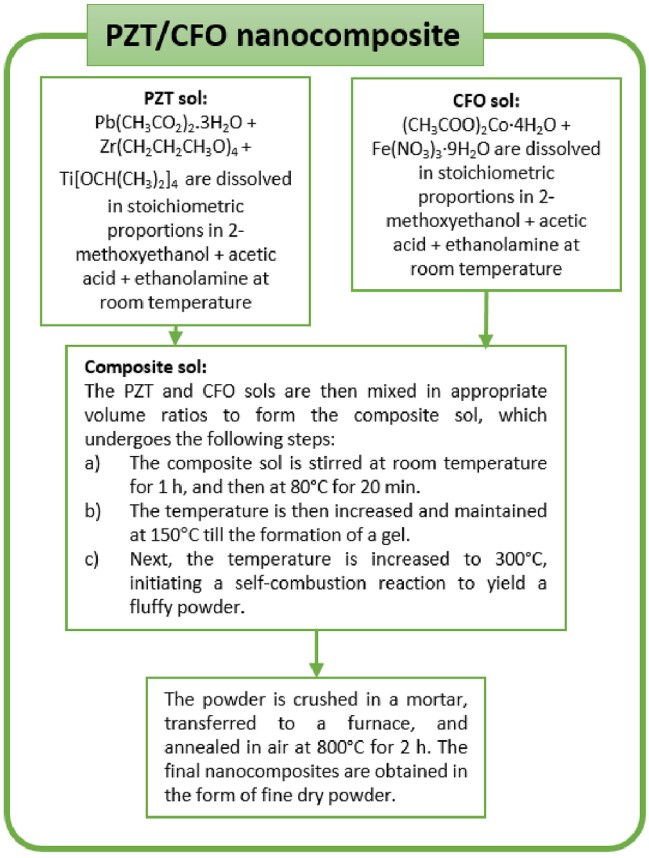

Fig. 1. Flow-chart showing the synthesis process of PZT/CFO nanocomposites. For more details, see text.

The annealed powder was pressed into cylindrical pellets for performing dielectric measurements. Both sides of the pellet were coated with conductive silver paste followed by slow drying. Ferroelectric hysteresis loops were measured at room temperature using a modified Sawyer-Tower circuit.

3. Results and discussion

3.1. Structural and morphological characterization

The XRD patterns of the synthesized samples are shown in Fig. 2. The reflections of CFO (Fig. 2a) and PZT (Fig. 2e) could by indexed to the cubic space group *Fd-3m* and tetragonal space group *P4mm*, respectively. The XRD patterns of the 50:50 and 75:25 nanocomposites (Fig. 2b and c) show reflections corresponding to both phases. The XRD pattern of the 95:05 nanocomposite (Fig. 2d) shows the reflections corresponding to the PZT phase only because of the very small % of CFO in this sample. Interestingly, we observe that the CFO nanoparticles in the nanocomposites have a smaller crystallite size than that in the pure phase. This can be seen in Fig. 2f and g, where we have compared the most intense reflection of the CFO phase in the XRD pattern of the pure sample with that in the 50:50 and 75:25 nanocomposites. Both the nanocomposites show broader peaks with respect to the pure sample indicating a smaller crystallite size of CFO in the former. We have previously observed a similar behavior in other nanocomposite systems [17].

TEM observations were performed to investigate the structure of the samples in more details. In particular, Fig. 3a shows a bright field image of the CFO powder. It is composed of nanocrystals having dimensions ranging from 40 to 300 nm. Selected area electron diffraction (SAED) measurements have revealed the presence of the cubic CFO phase only

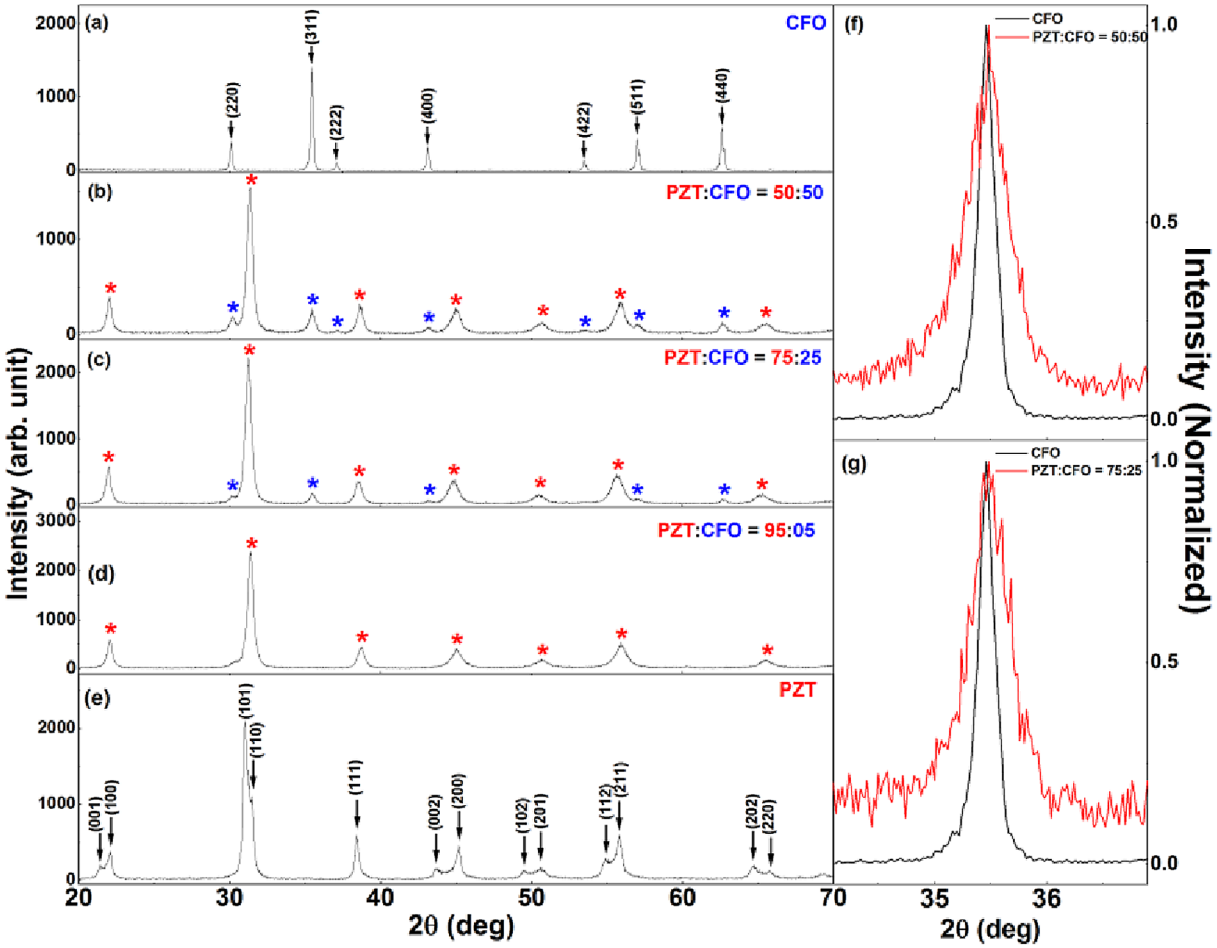

Fig. 2. Left: XRD patterns of (a) CFO, (b) PZT(50)/CFO(50) nanocomposite, (c) PZT(75)/CFO(25) nanocomposite, (d) PZT(95)/CFO(05) nanocomposite, and (e) PZT. Right: Normalized XRD patterns around the (3 1 1) peak for (f) CFO and PZT(50)/CFO(50) nanocomposite, and (g) CFO and PZT(75)/CFO(25) nanocomposite. The reflections corresponding to the CFO and PZT phases in the nanocomposite samples have been marked by blue and red asterisks, respectively. (For interpretation of the references to colour in this figure legend, the reader is referred to the web version of this article.)

(inset of Fig. 3a). The microstructure of the PZT(50)/CFO(50) nanocomposite is shown in Fig. 3b. The powder is composed of nanocrystals with dimensions that are typically smaller than in the CFO sample, ranging from 10 to 100 nm for both PZT and CFO phases. The lower dimension of the crystals is confirmed by SAED measurements. Indeed, a typical diffraction pattern of the sample, taken with the same selected area aperture used for the CFO sample, shows continuous diffraction rings instead of only distributed diffraction spots, as can be seen comparing the insets of Fig. 3a and b. This observation agrees with XRD data, revealing a smaller size of CFO grains in the nanocomposites with respect to that in pure CFO. Furthermore, it is important to stress that diffraction rings in the inset of Fig. 3b reveal the presence of both the

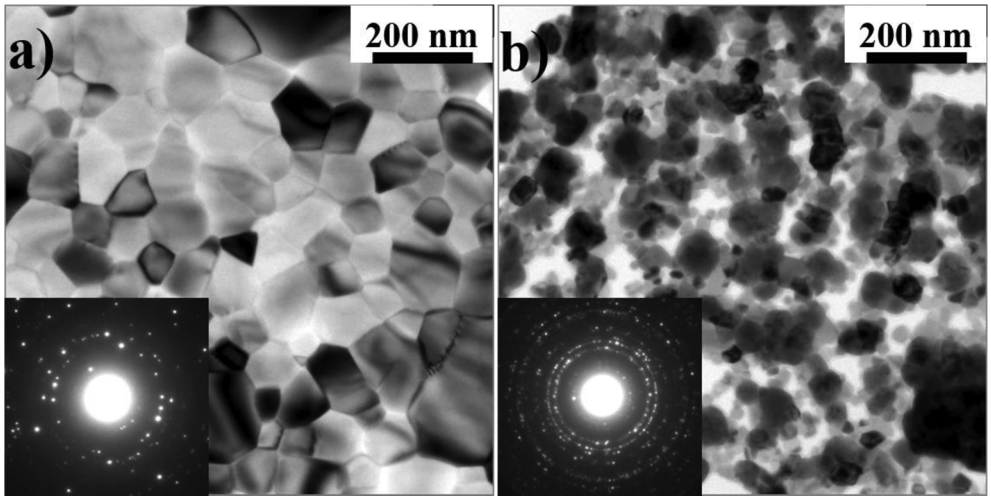

Fig. 3. TEM bright field images and corresponding SAED patterns (insets) of (a) CFO sample and (b) PZT(50)/CFO(50) nanocomposite.

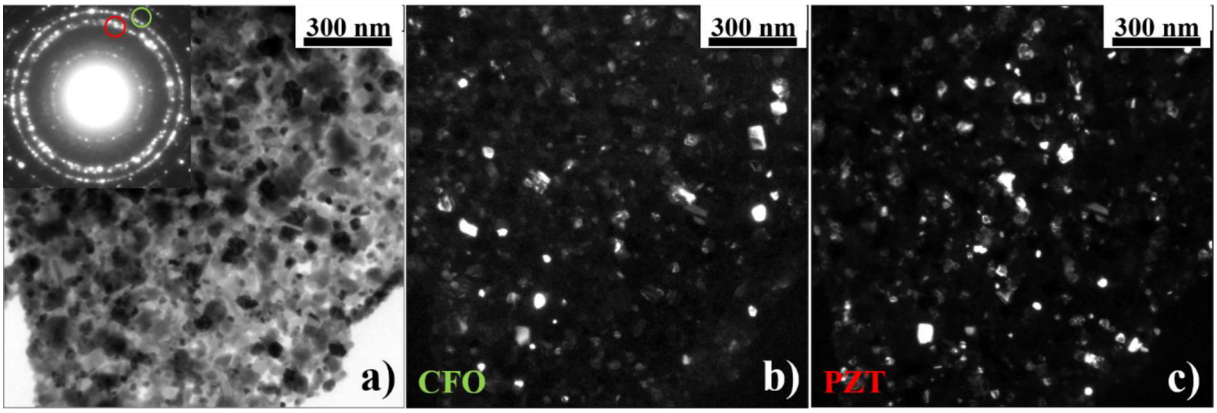

Fig. 4. PZT(50)/CFO(50) nanocomposite: (a) TEM bright field image and corresponding SAED patterns (inset), (b) dark field image showing CFO {1 3 1} grains (SAED, green circle), (c) dark field image showing PZT {1 0 1}/{1 1 0} grains (SAED, red circle). (For interpretation of the references to colour in this figure legend, the reader is referred to the web version of this article.)

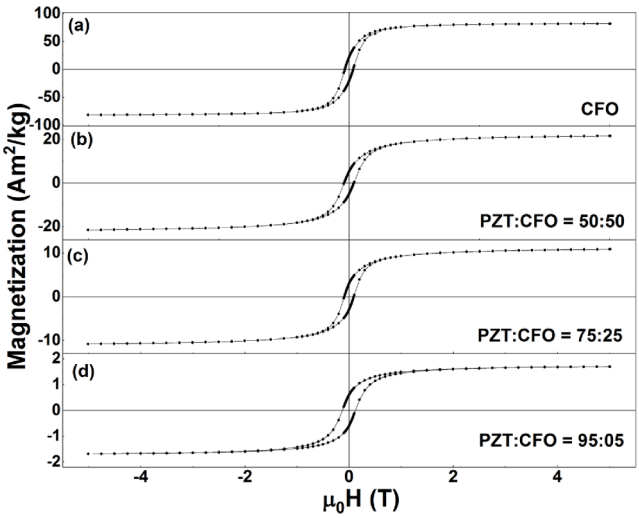

Fig. 5. Isothermal magnetization curves of (a) CFO, (b) PZT(50)/CFO(50) nanocomposite, (c) PZT(75)/CFO(25) nanocomposite, and (d) PZT(95)/CFO(05) nanocomposite at T = 300 K.

phases and TEM dark-field observations indicate a very good dispersion of one phase in the other. In particular, Fig. 4a shows a bright field image of the PZT(50)/CFO(50) sample with the corresponding SAED pattern in the inset. Fig. 4b and c are dark field images obtained with the objective diaphragm of the microscope selecting a portion of the CFO {1 3 1} diffraction ring (green circle in the SAED pattern), or a portion of the PZT {1 0 1} and {1 1 0} diffraction rings (red circle in the SAED pattern), respectively. In this way the CFO grains responsible for the selected diffraction intensity are lighted in the first case (Fig. 4b), while PZT grains are lighted in the second image (Fig. 4c). The distribution of CFO and PZT grains reveals a good dispersion of one phase in the other.

3.2. Magnetization measurements

Room temperature magnetic field dependent magnetization of CFO and the nanocomposite samples are shown in Fig. 5. We observe that the ferrimagnetic behavior of CFO is retained in the nanocomposite samples (even for a very low CFO fraction of only 5%), with the magnetization showing open hysteresis loops and near saturation for $\mu_0 H > 1$ T. The coercivity values of the samples are very similar, with the nanocomposites showing slightly higher values ($\mu_0 H_{C(\text{Composite; T = 300 K})}$ ranging from ~0.09 to 0.13 T) compared to that of pure CFO ($\mu_0 H_{C(\text{CFO; T = 300 K})} \sim 0.08$ T). This slightly larger coercivity of the nanocomposites compared to that of pure CFO can be due to the change in magnetic anisotropy of the CFO phase due to its reduced particle size in the nanocomposites.

3.3. Dielectric measurements

Fig. 6 shows the polarization versus electric field loop (P-E loops) recorded at room temperature and at a frequency of 50 Hz for PZT

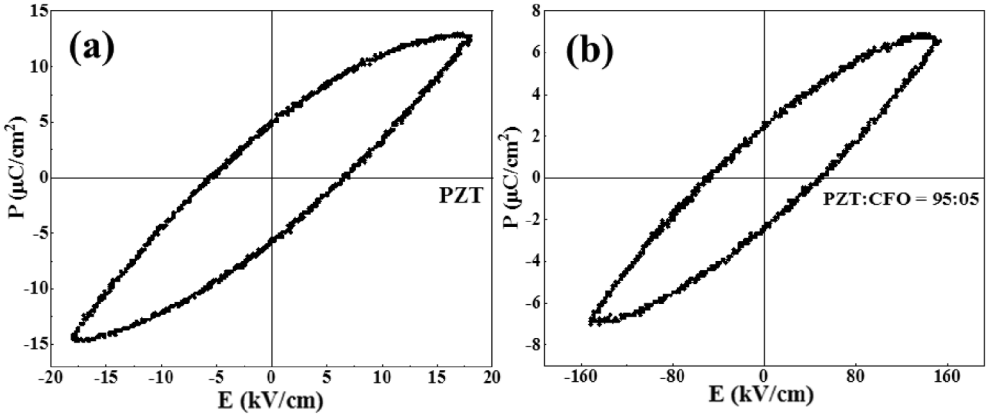

Fig. 6. Polarization versus electric field loop (P-E loops) recorded at room temperature and at a constant frequency of 50 Hz for (a) PZT and (b) PZT(95)/CFO(05) nanocomposite.

(Fig. 6a) and PZT(95)/CFO(05) nanocomposite (Fig. 6b). While such dielectric data should be investigated in detail [18], we note that the observed hysteresis loops are partially saturated, as have been reported previously for ferroelectric nanoparticles and their composite systems [19]. For the PZT sample, we obtain saturation polarization P_S and remanent polarization P_R values of ~12.7 μC/cm^2 and ~4.9 μC/cm^2, respectively. The incorporation of 5% CFO inside the PZT matrix leads to a decrease in the P_S (~6.7 μC/cm^2) and P_R (~2.5 μC/cm^2) values. Interestingly, recent studies have shown that for practical applications, for example, to operate multiferroic devices at a reduced energy consumption, it is necessary to design optimized materials with decreased polarization of values of ~5 μC/cm^2 [20]. This predicted value (5 μC/cm^2) is very close to what we observe in our PZT(95)/CFO(05) nanocomposite. In addition, the coercive field (E_C ~8 kV/cm for PZT) increases significantly after the incorporation of CFO inside the PZT matrix (E_C ~40 kV/cm for PZT(95)/CFO(05) nanocomposite). Similar behavior of P_S, P_R, and E_C were observed in their bulk counterparts [21]. The smaller values of P_S and P_R in the present case are associated with the reduced particle size of the nanocrystals as compared to bulk samples. For the samples with higher fraction of CFO phase, asymmetrical P-E loops were observed, which is mainly due to the domination of leakage current and non-linear dielectric effects caused by the conductive CFO phase.

4. Conclusions

In summary, we have synthesized PZT/CFO multiferroic nanocomposites using a new composite sol-based synthesis technique that yields homogeneous samples with enhanced interfacial coupling. This allows the possibility to design materials with improved coupling between the two phases. We have demonstrated phase purity of the synthesized samples, with no evidence of any undesired secondary phases. Room temperature investigations of the magnetic and dielectric properties of the samples reveal the desired functionalities in the nanocomposites with the simultaneous occurrence of open M vs H and P vs E loops. Our work demonstrates a new and effective synthesis technique that can be used to design functional nanocomposites with tunable magnetic and electrical properties.

CRediT authorship contribution statement

G. Kotnana: Investigation, Validation. **F. Sayed:** Investigation, Validation. **D.C. Joshi:** Investigation, Validation, Writing - original draft. **G. Barucca:** Investigation, Formal analysis, Writing - original draft, Visualization, Writing - review & editing. **D. Peddis:** Writing - review & editing. **R. Mathieu:** Writing - review & editing, Funding acquisition. **T. Sarkar:** Conceptualization, Methodology, Investigation, Validation, Formal analysis, Writing - original draft, Visualization, Writing - review & editing, Supervision, Project administration, Funding acquisition.

Declaration of Competing Interest

The authors declare that they have no known competing financial interests or personal relationships that could have appeared to influence the work reported in this paper.

Acknowledgements

We thank Stiftelsen Olle Engkvist Byggmästare (grant numbers 188-0179 and 184-546), Swedish Research Council (including VR starting grant number: 2017-05030), Carl Tryggers Stiftelse för Vetenskaplig Forskning (grant number KF 17:18), and the Royal Physiographic Society of Lund (the Märta and Eric Holmberg Endowment) for financial support.

References

[1] J. Ma, J. Hu, Z. Li, C.-W. Nan, Recent progress in multiferroic magnetoelectric composites: from bulk to thin films, Adv. Mater. 23 (2011) 1062–1087.
[2] G. Sreenivasulu, H. Qu, G. Srinivasan, Multiferroic oxide composites: synthesis, characterization and applications, Mater. Sci. Technol. 30 (2014) 1625–1632.
[3] H. Palneedi, V. Annapureddy, S. Priya, J. Ryu, Status and perspectives of multiferroic magnetoelectric composite materials and applications, Actuators 5 (2016) 9.
[4] Z. Chu, M. PourhosseiniAsl, S. Dong, Review of multi-layered magnetoelectric composite materials and devices applications, J. Phys. D: Appl. Phys. 51 (2018) 243001.
[5] L.A. Makarova, Y.A. Alekhina, A.S. Omelyanchik, D. Peddis, V.V. Spiridonov, V.V. Rodionova, N.S. Perov, Magnetorheological foams for multiferroic applications, J. Magn. Magn. Mater. 485 (2019) 413–418.
[6] W. Prellier, M.P. Singh, P. Murugavel, The single-phase multiferroic oxides: from bulk to thin film, J. Phys.: Condens. Matter 17 (2005) R803–R832.
[7] Y. Wang, J. Hu, Y. Lin, C.-W. Nan, Multiferroic magnetoelectric composite nanostructures, NPG Asia Mater. 2 (2010) 61–68.
[8] D. Halley, N. Najjari, H. Majjad, L. Joly, P. Ohresser, F. Scheurer, C. Ulhaq-Bouillet, S. Berciaud, B. Doudin, Y. Henry, Size-induced enhanced magnetoelectric effect and multiferroicity in chromium oxide nanoclusters, Nat. Commun. 5 (2014) 3167.
[9] G. Muscas, P.A. Kumar, G. Barucca, G. Concas, G. Varvaro, R. Mathieu, D. Peddis, Designing new ferrite/manganite nanocomposites, Nanoscale 8 (2016) 2081–2089.
[10] T. Sarkar, G. Muscas, G. Barucca, F. Locardi, G. Varvaro, D. Peddis, R. Mathieu, Tunable single-phase magnetic behavior in chemically synthesized $AFeO_3$-MFe_2O_4 (A = Bi or La, M = Co or Ni) nanocomposites, Nanoscale 10 (2018) 22990–23000.
[11] F. Sayed, G. Muscas, S. Jovanovic, G. Barucca, F. Locardi, G. Varvaro, D. Peddis, R. Mathieu, T. Sarkar, Controlling magnetic coupling in bi-magnetic nanocomposites, Nanoscale 11 (2019) 14256–14265.
[12] F. Sayed, G. Kotnana, G. Barucca, G. Muscas, D. Peddis, R. Mathieu, T. Sarkar, $LaFeO_3$-$CoFe_2O_4$ bi-magnetic composite thin films prepared using an all-in-one synthesis technique, J. Magn. Magn. Mater. 503 (2020) 166622.
[13] V. Mameli, A. Musinu, A. Ardu, G. Ennas, D. Peddis, D. Niznansky, C. Sangregorio, C. Innocenti, N.T.K. Thanh, C. Cannas, Studying the effect of Zn-substitution on the magnetic and hyperthermic properties of cobalt ferrite nanoparticles, Nanoscale 8 (2016) 10124–10137.
[14] B. Jaffe, R.S. Roth, S. Marzullo, Piezoelectric properties of lead zirconate-lead titanate solid-solution ceramics, J. Appl. Phys. 25 (1954) 809–810.
[15] K. Kakegawa, J. Mohri, S. Shirasaki, K. Takahashi, Sluggish pansition between tetragonal and rhombohedral phases of Pb(Zr, Ti)$_O$3 prepared by application of electric field, J. Am. Ceram. Soc. 65 (1982) 515–519.
[16] S. Nayak, T.K. Chaki, D. Khastgir, Spherical ferroelectric $PbZr_{0.52}Ti_{0.48}O_3$ nanoparticles with high permittivity: switchable dielectric phase transition with temperature, Ceram. Int. 42 (2016) 14490–14498.
[17] F. Sayed, G. Kotnana, G. Muscas, F. Locardi, A. Comite, G. Varvaro, D. Peddis, G. Barucca, R. Mathieu, T. Sarkar, Symbiotic, low-temperature, and scalable synthesis of bi-magnetic complex oxide nanocomposites, Nanoscale Adv. 2 (2020) 851.
[18] J.F. Scott, J. Phys. Condens. Matter 20 (2008) 021001.
[19] S. Liu, S. Xue, S. Xiu, B. Shen, J. Zhai, Surface-modified $Ba(Zr_{0.3}Ti_{0.7})O_3$ nanofibers by polyvinylpurrolidone filler for poly(vinylidene fluoride) composites with enhanced dielectric constant and energy storage density, Sci. Rep. 6 (2016) 26198.
[20] S. Manipatruni, D.E. Nikonov, C.-C. Lin, T.A. Gosavi, H. Liu, B. Prasad, Y.-L. Huang, E. Bonturim, R. Ramesh, I.A. Young, Scalable energy-efficient magnetoelectric spin-orbit logic, Nature 565 (2019) 35–43.
[21] Dipti, J.K. Juneja, S. Singh, K.K. Raina, C. Prakash, Enhancement in magnetoelectric coupling in PZT based composites, Ceram. Int. 41 (2015) 6108–6112.